Environmental Science and Pollution Research (2023) 30:71154–71170
https://doi.org/10.1007/s11356-023-27409-z

RESEARCH ARTICLE

Immobilization of chromium ore processing residue by alkali-activated composite binders and leaching characteristics

Guangjun Peng[1,2] · Pengpeng Zhang[1,2] · Linghao Zeng[1,2] · Lin Yu[1,2] · Dongwei Li[1,2]

Received: 5 January 2023 / Accepted: 30 April 2023 / Published online: 10 May 2023

Abstract

Chromium ore processing residue (COPR) is classified as hazardous solid waste because of the leachable Cr(VI). Cementitious materials are often used to solidify and stabilize heavy metals. However, most of them focus on the leaching concentration of particles after solidification and stabilization and lack research on leaching characteristics. This study investigated the leaching characteristics of heavy metals in three simulated environments (HJ557-2010, HJ/T299-2007, TCLP) after immobilizing COPR with composite binders. Industrial solid waste coal fly ash and lead–zinc smelting slag are used to prepare composite binders through alkali activation technology. Compressive strength, particle leaching toxicity, acid neutralization capability, and semi-dynamic leaching test are used to evaluate the performance of the solidified body. The solidified body can be applied to building materials or treated as general industrial waste. Heavy metals are mainly released from the matrix by surface washing at a low rate. The analysis results, including XRD, FTIR, and SEM–EDS, show that chemical binding and physical encapsulation are the main immobilizing mechanisms to realize the coordinated disposal of Zn and Cr(VI).

Keywords Solidification/stabilization · Diffusion coefficient · Semi-dynamic leaching test · Leaching mechanism

Introduction

Chromium and chromium salts are widely used in chemical metallurgy, leather, and electroplating anti-corrosion industries (Agrawal et al. 2006; Bratovcic et al. 2022). Chromium ore processing residue (COPR) is an industrial waste generated during the production of chromium salts. It is classified as hazardous waste because it contains Cr(VI), which is extremely toxic and carcinogenic (Chrysochoou et al. 2010; Shanker and Venkateswarlu 2011; Du and Chrysochoou 2020). In China, COPR must be disposed properly because it is listed as a national hazardous waste under No.261–041-21 in the HW21 series. The soda ash roasting chromium method has gained popularity due to its three times lower residue volume when compared to the conventional limestone roasting process. However, the residue still contains 1130–8500 mg/kg Cr(VI) since incomplete leaching (Sun et al. 2021). Therefore, it is necessary to dispose COPR safely and effectively.

Electrochemical techniques (Yu et al. 2022), biological approaches (Majee et al. 2021), and solidification/stabilization (S/S) (Rha et al. 2000; Shi and Fernández-Jiménez 2006) are broadly applied to dispose of COPR. S/S is considered an economic and effective disposal method in Europe and the USA due to technical feasibility and economy (Chrysochoou and Dermatas 2006; Gao et al. 2020). S/S together with binders are used extensively in the disposal of COPR, reducing the leaching toxicity of heavy metals through physical sequestration and chemical bonding, and transforming hazardous waste into insoluble, low migration, and low toxicity forms (Kanchinadham et al. 2015; Huang et al. 2018; Muhammad et al. 2019; Xia et al. 2020). Portland cement (PC) is a commonly used binder for S/S (Singh and Pant 2006; Chrysochoou and Dermatas 2006). However, PC generates significant energy consumption (up to 5000 MJ/t), non-renewable resources (limestone and clay 1.5t /t), and greenhouse gas (0.95 t/t) (Chen and Li 2011). New green bonding agents are urgently needed to replace

Responsible Editor: Ioannis A. Katsoyiannis

✉ Dongwei Li
litonwei@cqu.edu.cn

[1] State Key Laboratory of Coal Mine Disaster Dynamics and Control, Chongqing University, Chongqing 400044, China

[2] College of Resource and Safety Engineering, Chongqing University, Chongqing 400044, China

traditional PC. Binder materials are made from more sustainable industrial byproducts such as coal fly ash (FA) and blast furnace slag (Chen and Li 2011; Komljenović et al. 2020). Alkali-activated binder materials are becoming an alternative to PC for their superior durability and environmental friendliness (A et al. 2008; Pacheco-Torgal et al. 2008). Huang et al. (2018) used FA, blast furnace slag, and metakaolin to prepare alkali-activated cementitious materials for solidifying COPR and achieved a good immobilization effect. Salihoglu (2014) used FA and clay minerals to prepare alkali-activated geopolymer cementing materials for S/S of hazardous waste containing antimony. The products can be handled as general industrial solid waste after safe disposal. The aluminosilicate in FA undergoes depolymerization, recombination, and polycondensation reaction after the Si–O bond and Al-O bond are attacked by OH^- under the alkali activation, forming the geopolymer gelling product (Palomo 2003; Guo et al. 2010; Belviso 2018; Komljenović et al. 2020). However, a large amount of quartz, mullite, and other crystal components seriously reduce the alkali activation activity of FA (Guo et al. 2010; Görhan and Kürklü 2014; Zhang et al. 2014; Cho et al. 2017, p. 20; Nath 2019). Additional active silicon and aluminum sources were used to prepare composite geopolymer binders to overcome this problem. The geological polymerization of fly ash was enhanced by zinc slag rich in vitreous components. The isothermal calorimetry curve shows that adding zinc slag to the reaction system increases the exothermic peak of dissolution and polycondensation. (Nath 2019).

Lead and zinc smelting slag (LZSS) is a type of industrial waste from the non-ferrous smelting industry, with more than 32 million tons of smelting slag generated in China each year (Li et al. 2016). The particles form an amorphous glass phase that is easily activated by alkali, thanks to the incomplete energy released by the LZSS during high-temperature melting and water quenching. Zhang et al. (2020) used the alkali-activation technique to achieve self-cementation of LZSS and effective S/S of heavy metals Zn, Pb, Cu, and Cr. Luo et al. (2022a) used LZSS for the co-disposal of municipal waste incineration fly ash, with an immobilization efficiency of over 99% for Zn, Pb, and Cu. Water treatment residues are co-disposed by LZSS and gypsum sludge mixture, which can effectively stabilize As, Pb, and Zn in the residues under low PC usage, and the solidified body meets the performance of conventional building materials (Li et al. 2016). In summary, LZSS has good alkali-activated gelation properties and can provide active SiO_2 and Al_2O_3 for the activation reaction process. It can be seen that it is feasible to prepare an FA-LZSS-based composite binder with alkali activation technology and use it to solidify and stabilize COPR.

In the existing methods for fixed treatment of heavy metals, almost all make only a short leaching reference to assess the S/S capacity of the binder materials. The leaching concentration of heavy metals from binder materials was below the leaching toxicity standard (Rha et al. 2000; Li et al. 2016; Xia et al. 2019; Luo et al. 2022a). Simulated environment leaching experiments on solidified bodies have been performed using finely ground particles (< 9.5 mm), such as the toxicity characteristic leaching procedure (TCLP) and HJ/T299-2007 (Tang et al. 2017), which do not consider the reduction in leaching concentration due to the monolithic nature of the material. More importantly, it is necessary to confirm how heavy metals are released from the cement matrix. The experiments were classified as single extraction tests (e.g., TCLP, HJ/T299-2007, and EN12457 (Institution) (2003)) and dynamic leaching tests (e.g., US EPA multistage extraction tests, ANSI/ANS-16.1–2003, and ASTM C1308-08 (2008)) depending on whether the extracts were updated (Dermatas et al. 2004; Gao et al. 2020). Dynamic leaching tests provide a more realistic simulation of the actual leaching environment required for encapsulating contaminants in solidified matrices.

This study uses industrial waste FA and LZSS as raw materials to prepare alkali-activated composite binders for the disposal of COPR. The release characteristics of heavy metals Cr(VI) and Zn from the solidified matrix were investigated. According to ASTM C1308-08, three different leaching environments were selected to evaluate the stability of the solidified bodies, which are (1) running water used to simulate groundwater or surface water environment, the reference standard is HJ557-2010; (2) simulating the leaching process of heavy metals from the binder material under the effect of acidic rainfall, the reference standard is HJ/T299-2007; (3) TCLP in the US EPA 1311 was used to simulate a landfill leachate environment. The compressive strength, acid neutralization capacity, and environmental stability of binders were determined. The mineralogical components were characterized by X-ray diffraction (XRD), Fourier transforms infrared spectroscopy (FTIR), and scanning electron microscope and energy dispersion spectrum (SEM–EDS). This work provides a theoretical reference for the recycling of general industrial solid waste and the safe disposal of hazardous waste.

Materials and methods

Materials and sample preparation

The raw materials include two types of FA, LZSS and COPR. The FAs were obtained from a coal-fired power plant in Chongqing and classified as F (CaO wt% = 2.68% < 10%) and C (CaO wt% = 14.92% > 10%) according to GB/T 50146–2014. LZSS was taken from a lead–zinc smelter in Yunnan Province to improve the bonding properties of the

Table 1 Chemical composition of raw materials

Oxide	SiO_2	Al_2O_3	Fe_2O_3	CaO	MgO	SO_3	K_2O	Na_2O	TiO_2	ZnO	Cr_2O_3	PbO	Other
FFA	53.33	34.70	3.52	2.68	0.64	0.70	1.65	0.38	1.63	–	–	–	0.77
CFA	44.93	27.44	5.37	14.92	1.31	0.74	2.56	0.61	1.52	–	–	–	0.59
LZSS	32.78	11.29	35.69	10.03	2.58	2.24	–	0.76	0.74	2.19	–	0.22	1.48
COPR	1.80	24.32	45.67	0.11	8.97	0.12	–	3.93	1.32	0.13	12.39	-	1.24

alkali-activated composite binders. COPR was obtained from a chemical factory in Chongqing, China, which uses a soda ash roasting process to produce chromium salt. Table 1 shows the chemical composition of raw materials. It can be found that except for COPR, the other three contain a large amount of SiO_2, among which FA also contains more Al_2O_3, both of which happen to form geopolymer binders under the alkali-activated reaction. CaO is mainly concentrated in CFA and LZSS. In contrast, 91.35% of COPR comprises Al_2O_3, Fe_2O_3, MgO, and Cr_2O_3.

The leaching concentration and total amounts are important risk assessment indicators. As shown in Table 2, the leaching analysis of Zn^{2+} in LZSS showed that the concentration in the TCLP was as high as 124.63 mg/L. Although there is no uniform regulation on the leaching limit of Zn in the existing standards, its trace element in LZSS reached 9418 mg/kg revealing that its toxicity is serious. The leaching concentration of Pb in LZSS is very low, and the trace element is only 35 mg/kg, so its influence is ignored in the experiment. The leaching concentrations of Cr(VI) in TCLP and HJ/T299-2010 were 44.96 mg/L and 80.16 mg/L, respectively, which reached 9 and 16 times the limit values of 5.0 mg/L stipulated by GB5085.3–2007 and EPA.1311.

The XRD patterns of the raw materials are characterized in Fig. 1, where FFA (Fig. 1a) and CFA (Fig. 1b) have strong mullite and quartz crystalline peaks. These components hardly react and do not dissolve during the alkali activation process, resulting in a single FA as a raw material with almost no hardening properties under alkali-activated conditions (Chao et al. 2011; Nath 2019). The XRD pattern of LZSS (Fig. 1c) shows obvious dispersion peaks between 20 and 30° in the amorphous phases. Amorphous phases are the source of activity of the alkali-activated binders. In contrast, there is almost no dispersion peak in the XRD spectrum of COPR, and the iron-rich and chromium-rich crystalline phases corresponding to XRF are obvious.

The optimum quality ratios of LZSS to FFA and CFA in the composite binder were 0.2 and 0.3, respectively, obtained in the preliminary experiments using compressive strength and Zn^{2+} leaching concentration as indicators. The doping amounts (COPR/total mass) of solidified COPR in the composite binders were 10%, 20%, 30%, 40%, and 50%, respectively. The alkali activator was prepared and aged 12 h in advance using NaOH (analytical grade) modified sodium silicate solution ($Na_2O{\cdot}3.3SiO_2$, analytical grade), with Na_2O equivalent of 8% and modulus of 1.0, based on this equivalent and modulus could adequately activate amorphous phases and not lead to efflorescence in the experiments(Fernández-Jiménez and Palomo 2005). The solidified body was prepared in four steps: (i) mix FA and LZSS evenly according to the mass ratio, then add COPR in the way of equal substitution; (ii) add the mixture into the alkali activation solution, stir it evenly, pour the slurry into the steel mold (Φ25 mm×H25 mm), and discharge the excess bubbles on the vibration table; (iii) place the mold with slurry in the curing box at the set temperature for the initial 24 h; (iv) after demolding, the specimen shall be cured at room temperature to the specified age of 28 days. Detailed experimental parameters are shown in Table 3.

Methods

Compressive strength and particle leaching experiment

The universal testing machine for mechanics of materials (AG-250-I) of Shimadzu company, Japan, was used to test the compressive strength of the specimens. The test procedure was carried out at 1 mm/min. The same batch of specimens was subjected to three tests, and the average was chosen as the final result. Debris from the compressive strength test was used as a toxic leaching test (particle size < 9.5 mm). The leaching concentration and total amount of heavy metals were determined by inductively coupled plasma optical emission spectrometer (ICP-OES, ICAP6300). The leaching procedures of the HJ/T299-2007 and TCLP are summarized as shown in Table 4. The following formula (1) determines the S/S efficiency of heavy metals:

$$\eta = \frac{k \times C_0 - C_k}{k \times C_0} \quad (1)$$

Table 2 Leaching concentration (mg/L) and total amounts (mg/kg) of heavy metals

Leaching concentration	Zn in LZSS	Pb in LZSS	Cr(VI) in COPR
TCLP	124.63	0.45	44.96
HJ/T299-2007	18.09	0.21	80.16
Total amounts	9418	35	1163.47

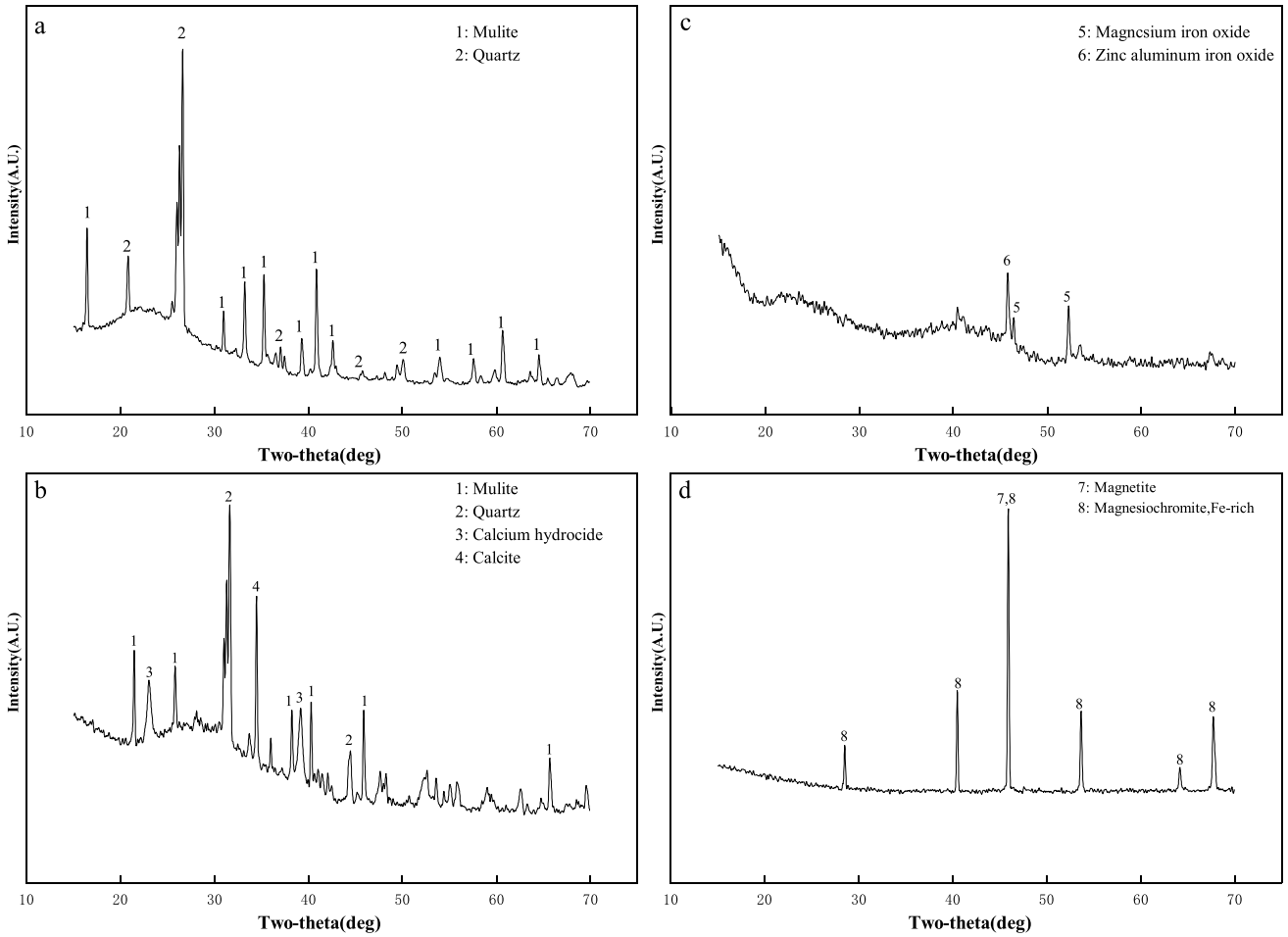

Fig. 1 Mineral composition of raw materials. (**a** FFA; **b** CFA; **c** LZSS; **d** COPR)

where k is the proportion of the doping COPR (%); C_0 is the leaching concentration in the raw material (mg/L); C_k is the leaching concentration in the composite binder (mg/L).

Table 3 Detailed experimental parameters

Samples ID	The proportion of raw materials (%)			Liquid–solid ratio	The temperature in the initial 24 h (°C)
	FA	LZSS	COPR		
F-L-COPR10[1]	72	18	10	0.30	40
F-L-COPR20	64	16	20		
F-L-COPR30	56	14	30		
F-L-COPR40	48	12	40		
F-L-COPR50	40	10	50		
C-L-COPR10[2]	63	27	10	0.32	40
C-L-COPR20	56	24	20		
C-L-COPR30	49	21	30		
C-L-COPR40	42	18	40		
C-L-COPR50	35	15	50		

[1]F-L-COPR10 = FFA-LZSS20-COPR10

[2]C-L-COPR10 = CFA-LZSS30-COPR10

The semi-dynamic leaching test

Solidified specimens were subjected to an ASTM C1308-08 semi-dynamic leaching test. Three leaching agents, HJ557-2010, HJ/T299-2007, and TCLP, were tested on solidified specimens containing 50 wt% COPR. The extractant volume to the surface area of the specimen was 10 mL/cm^2. The specimens were cleaned with distilled water before being immersed in the extractant to remove any surface contaminants. The update times of the extractant were 2 h, 5 h, and 1 day, and then, the update time was once a day until the 13th day. All leachates were measured for pH and the concentration of Zn^{2+} and Cr(VI). The final value was calculated by averaging the three test values.

The leaching behavior of heavy metals from cement-based materials is usually evaluated based on the effective diffusivity (Dermatas et al. 2004). The effective diffusion is calculated based on the semi-infinite medium model of Fick's diffusion theory (2008; Song et al. 2013). In this experiment, the mass of leachable heavy metals in LZSS and COPR is less than 20% of the total mass, so it is feasible

Table 4 Operating parameters of particle leaching toxicity experiment

Leaching environment	Extractant		Liquid–solid (mL/g)	Reversal (r/min)	Time (h) and temperature (°C)
	Solution	pH			
HJ/T299-2007	H_2SO_4: HNO_3 = 2:1 (mass ratio)	3.20 ± 0.05	10:1	30	18 + 23
TCLP	CH_3COOH	2.88 ± 0.05	20:1	30	18 + 23

to assume that the solidified body of the composite binder is a semi-infinite medium. When the diffusion coefficient is constant, the diffusion flux J of heavy metals at the solid/liquid interface in a semi-infinite medium varies with time t:

$$J = \sqrt{\frac{D_e}{\pi t}} \times C_0 = \sqrt{\frac{D_e}{\pi t}} \times \frac{M_0}{V} \tag{2}$$

The D_e = effective diffusion coefficient represents the diffusion and adsorption of substances in the matrix (cm^2/s), t = leaching time (s), C_0 = the heavy metal concentration in the specimen (mg/cm^3), M_0 = the mass of trace elements (mg), and V = the volume of the specimen (cm^3).

Equation (3) calculated the cumulative mass of Zn^{2+} and Cr(VI) at t in the leaching solution.

$$M_{n,i} = \sum C_i \times V_L \tag{3}$$

where $M_{n,i}$ is the cumulative mass of heavy metals after leaching time t (mg), $n = Zn^{2+}$ or Cr(VI), and i is the times of leaching solution update. C_i is the leaching concentration for the t time (mg/L); V_L is the volume of extractant (L).

Equation (4) calculates the cumulative fraction of heavy metal mass in the leaching solution after the leaching time t:

$$CFL = \frac{M_{n,i}}{M_0} \tag{4}$$

CFL is the cumulative mass fraction of heavy metal after leaching time t (%).

Equation (5) is used to calculate the effective diffusion coefficient:

$$D_e = \frac{\pi}{4} \times \frac{CFL^2}{t} \times \left(\frac{S}{V}\right)^2 \tag{5}$$

Acid neutralization capacity test

The acid neutralization capacity test (ANC) supports interpreting semi-dynamic leaching results. Specimens with 50 wt% COPR content was used for the ANC. The ANC test was performed according to the procedures established by Stegemann and Côté (1999). After testing the compressive strength, the debris was ground to a particle size of less than 100 µm. Distilled water was added at a liquid–solid ratio of 10. The powder-distilled water mixture slurry was titrated to the target pH (2, 3, 4, 5, 6, 7, 8, 9, 10) using 0.1 M HNO_3 solution. The leachate was filtered with 0.45 µm filter paper to determine the concentrations of Zn^{2+} and Cr(VI).

Characterization and analysis

XRD and FTIR analyzed the mineralogy of all specimens. XRD used CuKα radiation, working voltage 40 kV and current 30 mA, and scanning range of 10–70°. The molecular structures and chemical bonds were tested using the Thermo Scientific Nicolet iS50 infrared spectrometer under the following conditions: KBr tablet, resolution 4 cm^{-1}, and wave number from 4000 to 400 cm^{-1}. Thermos Scientific Quattro-S tested SEM–EDS at 20 kV operating voltage.

Results

Compressive strength analysis

Figure 2 shows the effect of COPR content on the 28-day compressive strength. Adding COPR decreases the compressive strength of composite binders, similar to the previous use of other cement materials that contained COPR (Huang et al. 2016; Xia et al. 2020; Yu et al. 2021). The addition of COPR reduced the content of active substances in the system. XRD of COPR reveals that it has almost no volcanic ash activity, and the crystal peak of chromite is strong. XRF revealed that the addition of COPR reduced the calcium content of the system, reducing the amount of C-S–H, C-A-S–H,[1] and other binder products. At the same time, excessive iron content hinders the gel phase formation in the solidified body, and the possible presence of rust will reduce the density of solidified body (Xia et al. 2019). Excessive heavy metals will produce more hydroxyl complex, which will consume more OH^- and weaken the dissolution of raw materials and hinder slurry fluidity, reducing silicon, and aluminum source transmission efficiency and directly inhibiting the polycondensation reaction of geopolymer gel (Wang et al. 2018). The higher calcium content in the CFA-LZSS system

[1] C-A-S–H in the cement product represents $CaO\text{-}Al_2O_3\text{-}SiO_2\text{-}H_2O$.

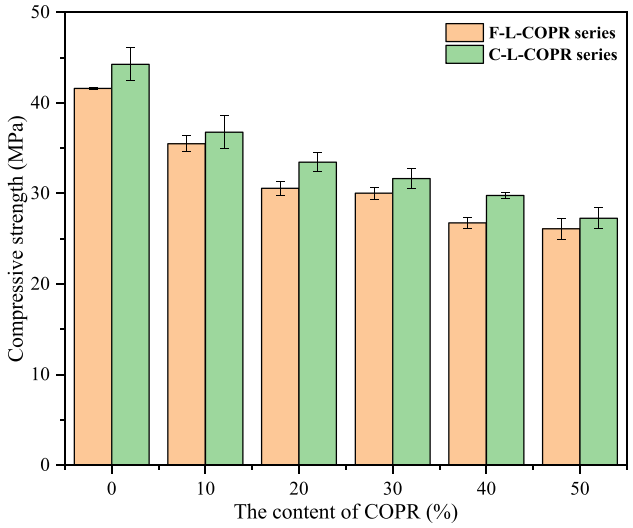

Fig. 2 Relationship between compressive strength of composite binder and COPR content

binders can effectively fix heavy metals in three ways: (1) N-A-S–H[2] geopolymer gel has a 3D network structure, which can "lock" heavy metal ions in the structure; (2) calcium-containing gels such as C-A-S–H and C-S–H support the compact structure of the solidified body, thereby reduces the contact between heavy metal ions and the external environment and hinders leaching migration; (3) the geopolymer gel is a three-dimensional network structure formed by the polymerization of neutral groups of silicon-oxygen tetrahedron [SiO4] and negatively charged aluminum oxygen tetrahedron [AlO4] by sharing oxygen atoms, so the positive charge of heavy metal ions can produce electrostatic action, to achieve the purpose of immobilization (Wang et al. 2018).

Acid neutralization capacity

The ANC test results reflect the acid buffering capacity of the matrix material. As shown in Fig. 3, before acid neutralization titration, C-L-COPR50 obtained a higher pH than F-L-COPR50 (i.e., 12.15 vs 12.05). Due to the calcium compounds being susceptible to acid corrosion and neutralization, the CFA-LZSS system has a higher pH in the initial solution (Song et al. 2013). Ca^{2+} exists in three forms in the binder: (1) free radical calcium ions in the void water, (2) adsorbed on the surface by the gel matrix in the form of $Ca(OH)_2$, and (3) participate in the hydration process to form calcium hydrates, such as C-S-H and C-A-S-H gel (Guo et al. 2010). Good linear fitting analysis can be carried out when the pH set by ANC is between 3 and 10. The absolute slope of Y_1 and Y_2 are 0.16 and 0.13, respectively, revealing that Y_2 has a better acid neutralization ability. The solubility

Table 5 Leaching concentration (mg/L) and S/S efficiency (%) of Zn^{2+} and Cr(VI)

Samples ID	HJ/T299-2007				EPA.1311 TCLP			
	Cr(VI)	Zn^{2+}	η (Cr(VI))	η (Zn^{2+})	Cr(VI)	Zn^{2+}	η (Cr(VI))	η (Zn^{2+})
F-L-COPR10	0.10	0.44	98.75	87.76	0.12	4.60	97.40	81.55
F-L-COPR20	0.42	0.46	97.38	87.29	0.14	3.83	98.50	84.63
F-L-COPR30	0.58	0.35	97.59	90.22	0.24	3.39	98.22	86.40
F-L-COPR40	0.63	0.41	98.04	88.81	0.28	3.06	98.41	87.72
F-L-COPR50	0.85	0.34	97.88	90.52	0.32	2.15	98.57	91.38
C-L-COPR10	0.33	0.13	95.83	97.64	0.07	0.87	98.42	97.68
C-L-COPR20	0.45	0.18	96.59	96.70	0.08	1.13	99.12	96.99
C-L-COPR30	0.61	0.14	97.45	97.38	0.10	1.00	99.26	97.33
C-L-COPR40	0.69	0.17	97.83	96.90	0.13	1.74	99.29	95.34
C-L-COPR50	0.71	0.20	98.24	96.37	0.22	1.16	99.03	96.89
Critical limits by GB5085.3–2007	5	100						
Critical limits by US.EPA.1311	2.5	–						

can generally accommodate more COPR. Whether CFA-LZSS or FFA-LZSS system, the solidified body strength can remain above 25 MPa, which still meets the requirement of building material strength (> 10 MPa) (Li et al. 2020).

Particle leaching toxicity analysis

Table 5 shows the heavy metals leaching concentrations and critical limits of Cr(VI) and Zn^{2+}. The leaching concentrations in simulated landfill leachate (TCLP) and simulated acid rain (HJ/T299-2007) were far below the critical limit values. The S/S efficiency of the composite binders on Cr(VI) was better than that of Zn^{2+}, possibly due to a large amount of Zn in LZSS (9418 mg/kg). The composite

[2] N-A-S–H in cement is Na_2O-Al_2O_3-SiO_2-H_2O.

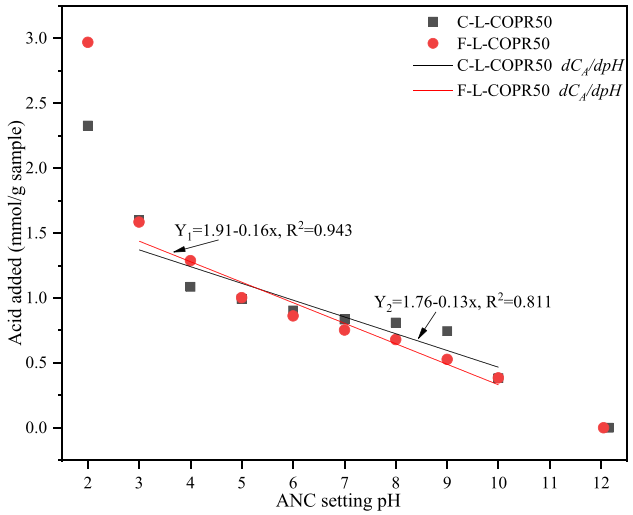

Fig. 3 Titration curves of 0.1 M HNO_3 for C-L-COPR50 and F-L-COPR50

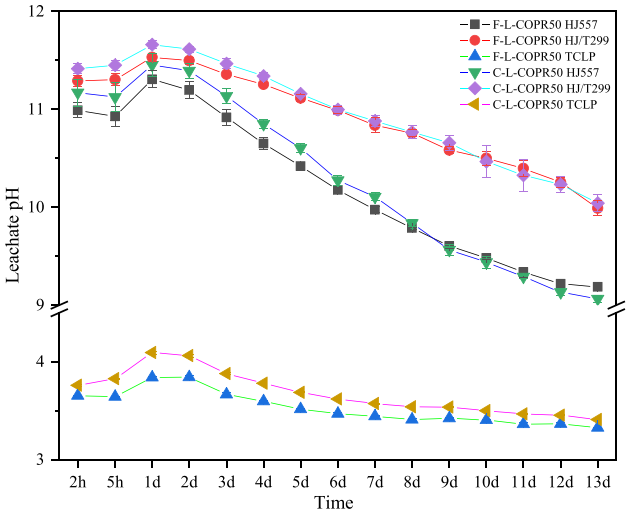

Fig. 5 The pH changes of leachate with time

of calcium-containing hydrates in an acidic environment is the reason for their high acid-neutralization ability.

The concentration of Cr(VI) and Zn^{2+} in the solution was determined after acid titration, as shown in Fig. 4. As the titration pH becomes more acidic, the concentration of heavy metals increases since the acidic environment destroys the structure of the composite binder and releases heavy metals. In general, C-L-COPR50 was more affected by an acidic environment than F-L-COPR50. This is related to the higher acid neutralization ability of C-L-COPR50. The structure of the binders is destroyed with the dissolution of calcium-containing gel and $Ca(OH)_2$. The sample of F-L-COPR50 can still maintain a low leaching concentration even in a strong acid environment, which can determine the effective immobilization of heavy metals by geopolymer gel.

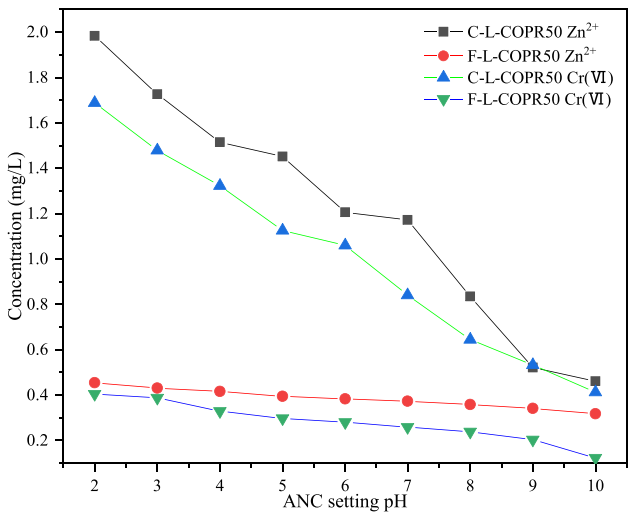

Fig. 4 Heavy metal concentration in acid titration solution

The semi-dynamic leaching test

Leachate pH

Figure 5 illustrates how the pH of leachate changes over time during the semi-dynamic leaching test. Compared with inorganic acids composed of H_2SO_4 and HNO_3, CH_3COOH can continuously release H^+ and neutralize alkaline substances, thus maintaining a low pH. HJ557 and HJ/T299 environments have a similar pH change before 3 days, but the sulfuric acid nitric acid solution has a higher pH in subsequent use. The experiment revealed the presence of black particles in the HJ/T299 leachate and suggested that the composite binder solidified body may have been dissolved.

Calculate the effective diffusion coefficient

The concentration of Cr(VI) and Zn^{2+} in a semi-dynamic leaching solution varies with time, as shown in Fig. 6. The leaching concentration of Cr(VI) increased gradually in the first 2 days and then decreased gradually. At the early stage of leaching, heavy metals on the surface of the solidified body are easily dissolved and released by direct contact with the solution. In the subsequent leaching cycle, the leaching of heavy metals is mainly affected by diffusion, and the composite binder's dense body hinders water infiltration into the interior. At the same time, the chemically fixed and physically wrapped heavy metals were effectively fixed so that the leaching concentration of hexavalent chromium gradually decreased. However, small cumulative mass fraction changes were detected, as shown in Fig. 7. The CFL value of Cr(VI)

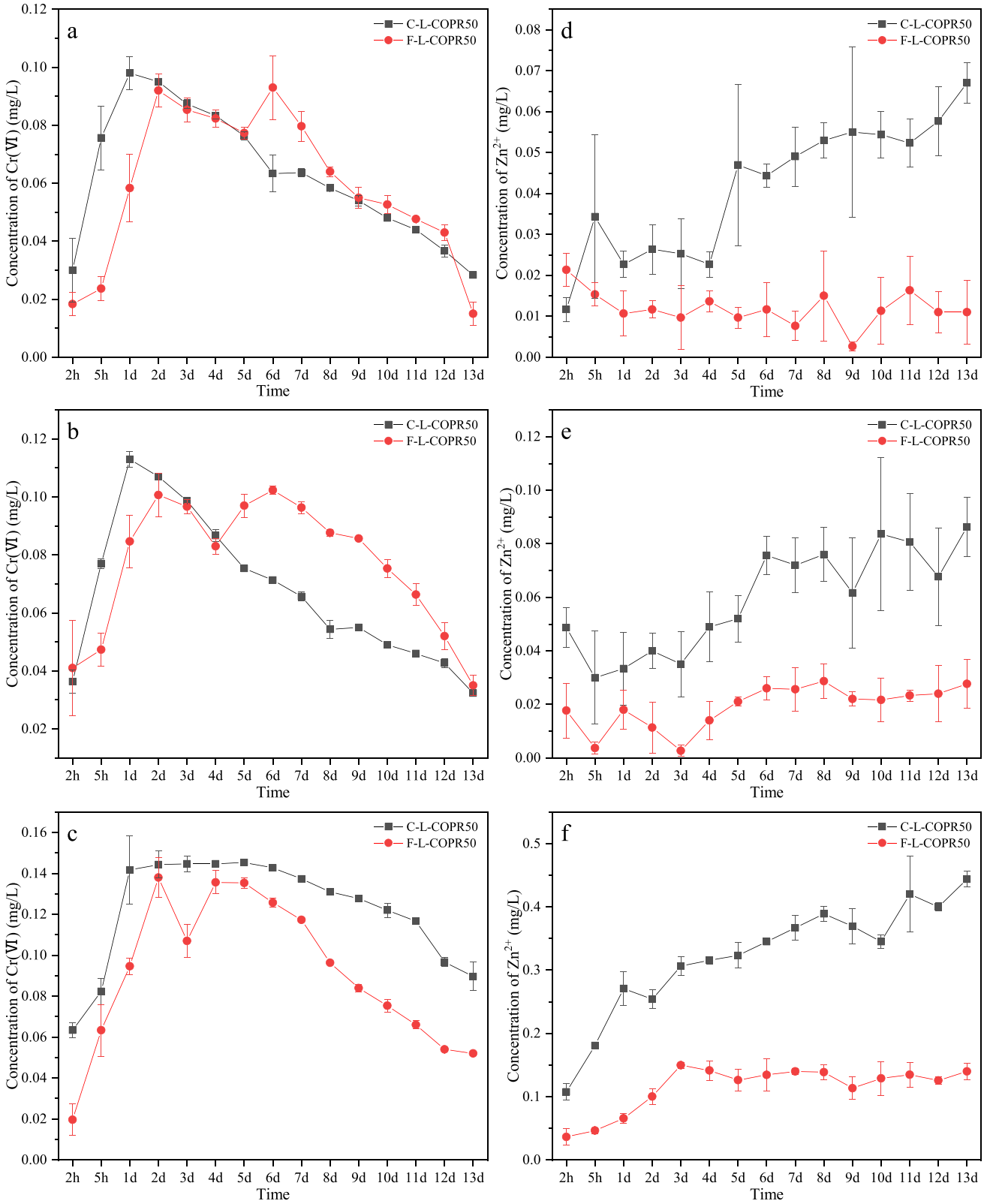

Fig. 6 Change of heavy metal leaching concentration with time. **a**, **b**, and **c** are Cr(VI) in HJ557, HJ/T299, and TCLP, respectively; **d**, **e**, and **f** are Zn^{2+} in HJ557, HJ/T299, and TCLP, respectively

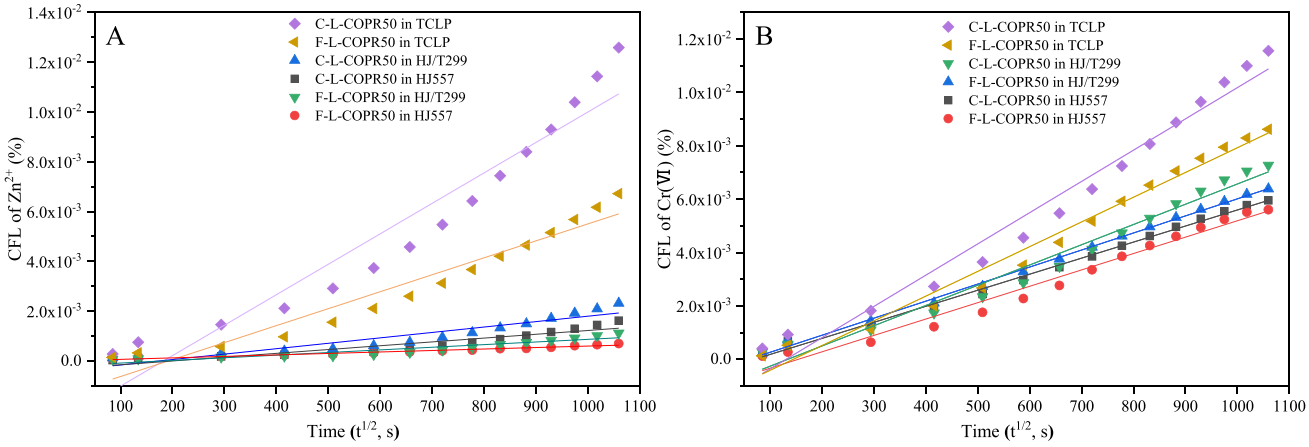

Fig. 7 The cumulative leaching mass fraction (CFL) as a function of $t^{1/2}$. **A** $Zn.^{2+}$; **B** Cr(VI)

was always the largest in the TCLP environment, which was related to the fact that the composite binder hardening body maintained a consistently high leaching concentration in TCLP environment (Fig. 6c). It is revealed that the strong acid environment more damages the structure of the composite binder. This phenomenon is also observed in Fig. 6f when the leaching concentration of Zn^{2+} is 1 order of magnitude higher than in Fig. 6 d and e.

In Fig. 6d–f, it can be found that the leaching concentration of F-L-COPR50 is always lower than that of C-L-COPR50, and the former can fix Zn^{2+} more effectively. It can be found that the surface leaching of specimens in the HJ557 environment is extremely low, the highest leaching concentration is in the TCLP environment, and the leaching concentration in the sulfuric acid solution is in the middle. This is also explained in "Environmental stability analysis," where the three types of environments did not cause excessive corrosion on the specimen F-L-COPR50, and the compressive strength was improved in the water curing.

The CFL of Cr(VI) and Zn^{2+} are shown in Fig. 7. It can be found that all of them have a good linear fit except C-L-COPR50 in the TCLP leaching environment. The slope of the linear fitting line increases with the increasing acidity of the leaching environment. This aligns with the diffusion characteristics of element leaching in solid materials. In any of the leaching environments, the slope of the fitted line of F-L-COPR50 is smaller than that of C-L-COPR50, which reflects that the former has better corrosion resistance and heavy metals immobilization ability.

To better explain the diffusion characteristics of heavy metals in the solidified body, Table 6 calculates the diffusion coefficient of each stage according to Eq. (5). According to the research results of Malviya and Chaudhary (2006), when $De < 3 \times 10^{-13}$ cm^2/s, the diffusion and migration rate of heavy metals from the binder can be considered very low. Table 6 shows the heavy metal leaching diffusivity in the composite binder reveals low mobility. The diffusion coefficient of F-L-COPR50 is generally lower than that of C-L-COPR50. Especially in a simulated acidic environment, the De value of F-L-COPR50 can even be 1 order of magnitude lower than that of C-L-COPR50, which makes it have better acid corrosion resistance and environmental stability. The negative logarithm of the diffusion coefficient (ρDe) represents the leaching rate of heavy metals from the matrix and the main leaching mechanism (Malviya and Chaudhary 2006). As shown in Table 6, all other specimens have good corrosion resistance. Heavy metal leaching occurs primarily through diffusion, except C-L-COPR50 in TCLP, where leaching occurs primarily led by dissolution. This is similar to the mechanism of dissolution occurring in an acetic acid environment found by Gao et al. (2020).

Environmental stability analysis

After semi-dynamic leaching experiments, excess water was removed in an oven at 40 °C. The compressive strength and mass loss were tested, as shown in Fig. 8. The mass loss of C-L-COPR50 in an acidic environment was found to be 5.42% and 4.12% in HJ/T299-2007 and TCLP, respectively. This is due to its high calcium content, and the calcium hydrates C-S–H gel and $Ca(OH)_2$ have strong degradability in an acidic environment (Yip et al. 2008; Wang et al. 2019). Compared with the high-calcium system, F-L-COPR50 has good acid and corrosion resistance, and its compressive strength is still maintained, even contributing to strength improvement under water curing (Poon et al. 1997). The low-calcium system forms a more cross-linked N-A-S–H binder, which gives it better corrosion resistance (Yip et al. 2008; Garcia-Lodeiro et al. 2011). EDS analysis of F-L-COPR50 also revealed lower calcium content (Fig. 14), while Na, Al, and Si were uniformly distributed in the sample. The low calcium system gel product N-A-S–H has

Table 6 Leaching diffusion coefficient (De, cm^2/s)

Samples		C-L-COPR50				F-L-COPR50			
Environments		HJ557-2010	HJ/T299-2007		TCLP	HJ557-2010	HJ/T299-2007		TCLP
Cr(VI)	Range	6.81×10^{-13}–4.41×10^{-12}		9.98×10^{-13}–5.02×10^{-12}	3.03×10^{-12}–1.62×10^{-11}	2.54×10^{-13}–4.00×10^{-12}	1.27×10^{-12}–6.54×10^{-12}		2.92×10^{-13}–9.07×10^{-12}
	Mean	3.59×10^{-12}		4.23×10^{-12}	1.04×10^{-11}	2.52×10^{-12}	4.30×10^{-12}		6.03×10^{-12}
	ρDe[1]	11.45		11.37	10.98	11.60	11.36		11.22
	Mobility	Average		Average	High	Average	Average		Average
	Mech.[2]	Diffusion		Diffusion	Dissolution	Diffusion	Diffusion		Diffusion
Zn^{2+}	Range	1.75×10^{-14}–3.19×10^{-13}		1.23×10^{-13}–6.54×10^{-13}	1.49×10^{-12}–1.92×10^{-11}	3.78×10^{-14}–1.55×10^{-13}	2.78×10^{-14}–1.53×10^{-13}		3.81×10^{-13}–5.48×10^{-12}
	Mean	1.34×10^{-13}		3.21×10^{-13}	9.02×10^{-12}	5.97×10^{-14}	7.45×10^{-14}		2.65×10^{-12}
	ρDe	12.87		12.49	11.04	13.22	13.13		11.58
	Mobility	Low		Average	Average	Low	Low		Average
	Mech	Surface wash		Diffusion	Diffusion	Surface wash	Surface wash		Diffusion

[1]The value of ρDe represents the leaching rate, and the higher the value, the slower the leaching rate. When ρDe < 11.0 represents high mobility, leaching is dominated by dissolution. Mean mobility occurs when 11.0 < ρDe < 12.5, and diffusion dominates. When ρDe > 12.5, low mobility occurs, which is dominated by washing on the surface of the specimen

[2]Mech: leaching mechanism

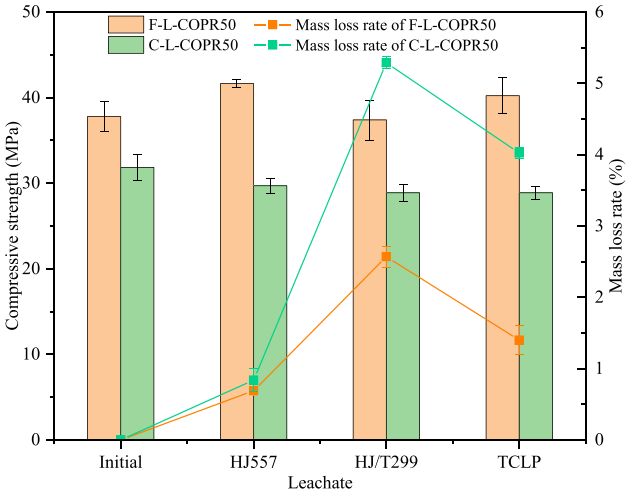

Fig. 8 Compressive strength and mass loss of specimens after semi-dynamic leaching test

strong corrosion resistance and a stronger immobilization for heavy metals.

The corrosion degree of the specimen after the semi-dynamic leaching experiment is shown in Fig. 9. It can be found that the composite binder is corroded obviously by sulfuric acid and nitric acid solution. The stability and surface integrity are good in the surface water and acetic acid solution environment. On the whole, C-L-COPR50 is more corroded than F-L-COPR50. Especially in HJ/T299, the C-L-COPR50 surface appears powder. On the one hand, it is due to the solubility of calcium hydrate in an acidic environment (Bakharev 2005; Ariffin et al. 2013). This can be reflected in the strong acid neutralization ability of C-L-COPR50. On the other hand, sulfate ions react with calcium hydrates to form gypsum ($CaSO_4•2H_2O$) and ettringite ($3CaO•Al_2O_3•3CaSO_4•32H_2O$), which have larger volumes and thus cause greater corrosion and destruction of the binder hardening body (Ariffin et al. 2013). The reaction equation between calcium hydrate and sulfate ion in an acidic environment is as follows:

$$Ca^{2+} + SO_4^{2-} + 2H_2O \rightarrow CaSO_4 \bullet 2H_2O \tag{6}$$

$$3SO_4^{2-} + 3Ca^{2+} + 3CaO \bullet Al_2O_3 \bullet 6H_2O + 26H_2O \rightarrow 3CaO \bullet Al_2O_3 \bullet 3CaSO_4 \bullet 32H_2O \tag{7}$$

XRD analysis

The mineralogy of the solidified body of COPR was analyzed, as shown in Fig. 10. Ca-Al-Si hydrate (#PDF 84–0945) was found in the XRD pattern of solidified bodies with low COPR content. These binder components are the

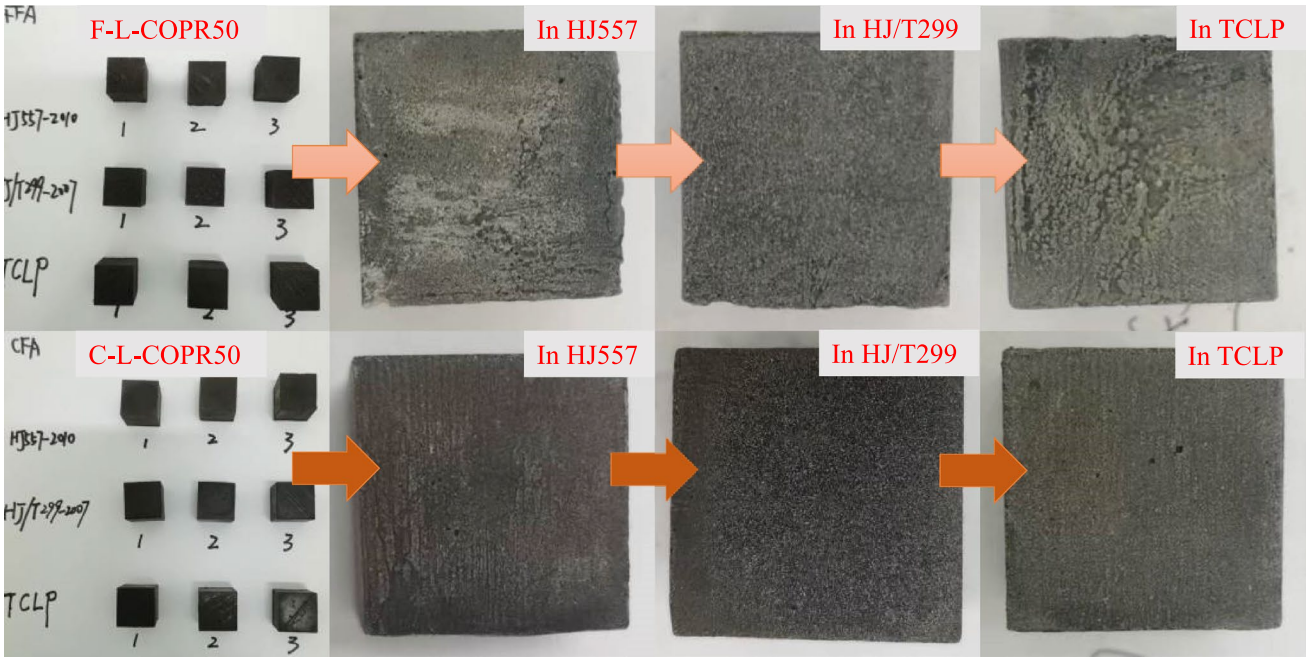

Fig. 9 The apparent changes of specimens in different environments

matrix of S/S heavy metals. Notably, the presence of spinel structures (spinel(Zn, Cr-exchanged)) was found in all samples, and the presence of zinc-chromium oxides ($ZnCr_2O_4$, #PDF 87–0028) may be the result of spinel dissolution and reconstruction in the composite binder (Xia et al. 2019; Zhang et al. 2020). The stable crystal structure explains the sample's high compressive strength and chemical stability, which can achieve stable chemical fixation of heavy metals (Wang et al. 2019). Magnesium iron ore different from raw material COPR (Fig. 1d) was observed in all samples, while chromium was not detected. Magnesite minerals were characterized by lower crystal peaks, which may be due to (1)

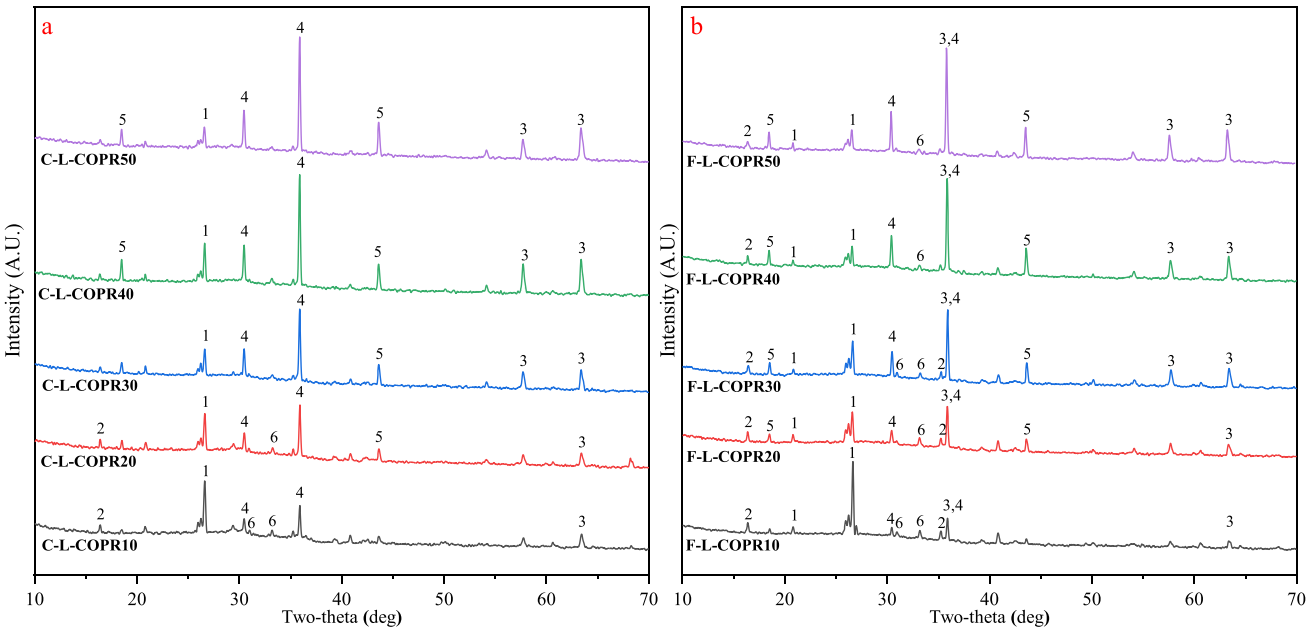

Fig. 10 XRD pattern of composite binder solidified bodies. **a** C-L-COPR series; **b** F-L-COPR series (1: quartz; 2: mullite; 3: Fe_2O_3; 4: spinel; 5: magnesium iron ore; 6: Ca-Al-Si hydrate)

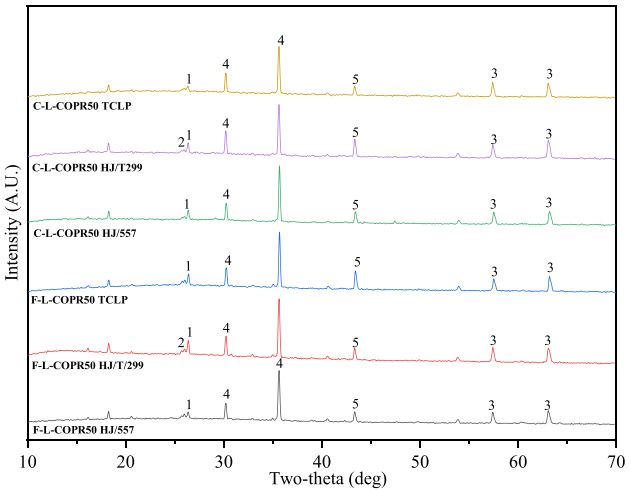

Fig. 11 XRD pattern after semi-dynamic leaching experiment (1: quartz; 2: gypsum; 3: Fe_2O_3; 4: spinel; 5: magnesium iron ore)

the mineral dissolved in an alkali solution and participated in geological polymerization and (2) the composite binder covering the mineral surface provided a physical barrier to the leaching of heavy metals Zn and Cr(VI). This phenomenon is also manifested in the weakening of quartz and mullite crystal peaks (Liu et al. 2018; Nath 2019).

Albite (#PDF 76–0927), Anorthite (#PDF 86–1707), Sub-mellite (#PDF 79–2423), and C-S–H gel phases were determined in C-L-COPR50. This is related to the fact that the raw material contains more calcium, providing more Ca^{2+} to participate in the reaction (Yip et al. 2008). In contrast, the products found in the F-L-COPR series samples are mainly the N-A-S–H phase (Thomsonite, #PDF 78–0296). These mineral phases reveal that the composite binder solidification and stabilization of heavy metals is the joint action of C-A-H, C-A-S–H, and N-A-S–H gels. The bond between the gel and the incomplete reaction particles supports the solidified body with a compact structure and mechanical properties.

As described in "Environmental stability analysis," it can be found that all specimens suffer different degrees of corrosion in an acidic environment. The mineralogical analysis in Fig. 11 of the composite binder after semi-dynamic leaching shows that except for the appearance of new phase gypsum in the HJ/T299 environment, the composition of other minerals hardly changes, demonstrating the stability of the composite binder. After a semi-dynamic leaching corrosion environment, acid corroded the incomplete reaction of the water compounds, thus releasing the encapsulated COPR raw materials, making the spinel mineral phase and hematite the main crystal phase.

FTIR analysis

Fourier transform infrared spectroscopy (FTIR) is widely used to study amorphous silica-aluminate structures because of its high sensitivity to short-range ordered structures (Zhang et al. 2008). The main band near 1000 cm^{-1} is caused by the stretching vibration of T-O (T = Si or Al) (band "c" in Fig. 12B and the band "3" in Fig. 12A), while the bending vibration of the O-Si–O bond in [SiO4] is caused by the wave number near 450 cm^{-1} (Guo et al. 2010; Garcia-Lodeiro et al. 2011). The Si–O-Si bond bending vibration in mullite is revealed in band "b" of Fig. 12B, explaining that the crystals of mullite and quartz hardly participate in the alkali activation reaction (Nath 2019). A more intense mullite crystal peak characterized in Fig. 10b is confirmed. Compared with the C-L-COPR series, the addition of COPR has a greater impact on the structure

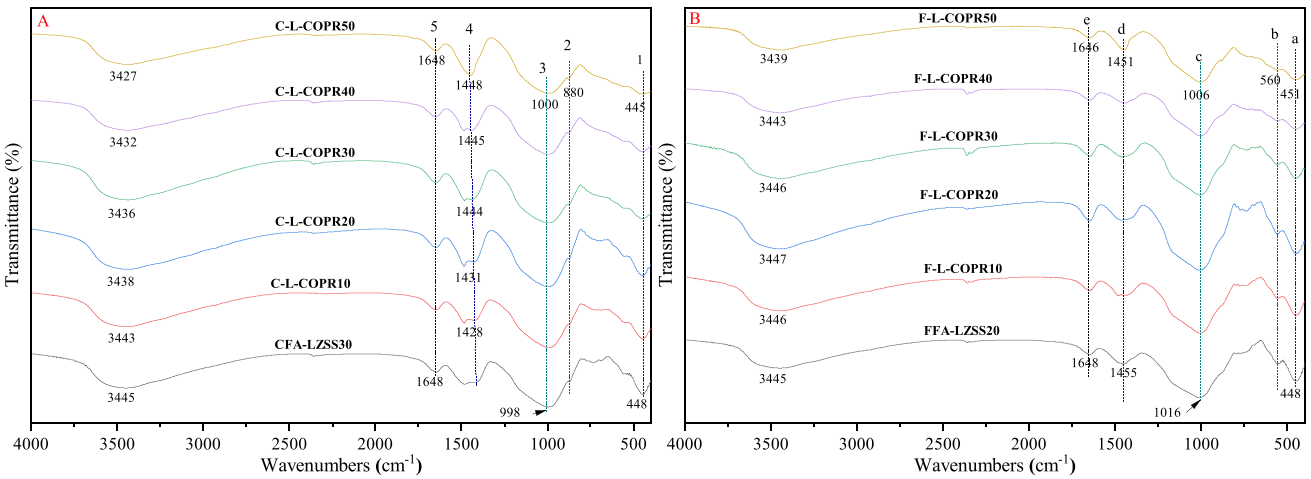

Fig. 12 FTIR spectra of composite binder solidified body. **A** C-L-COPR series; **B** F-L-COPR series

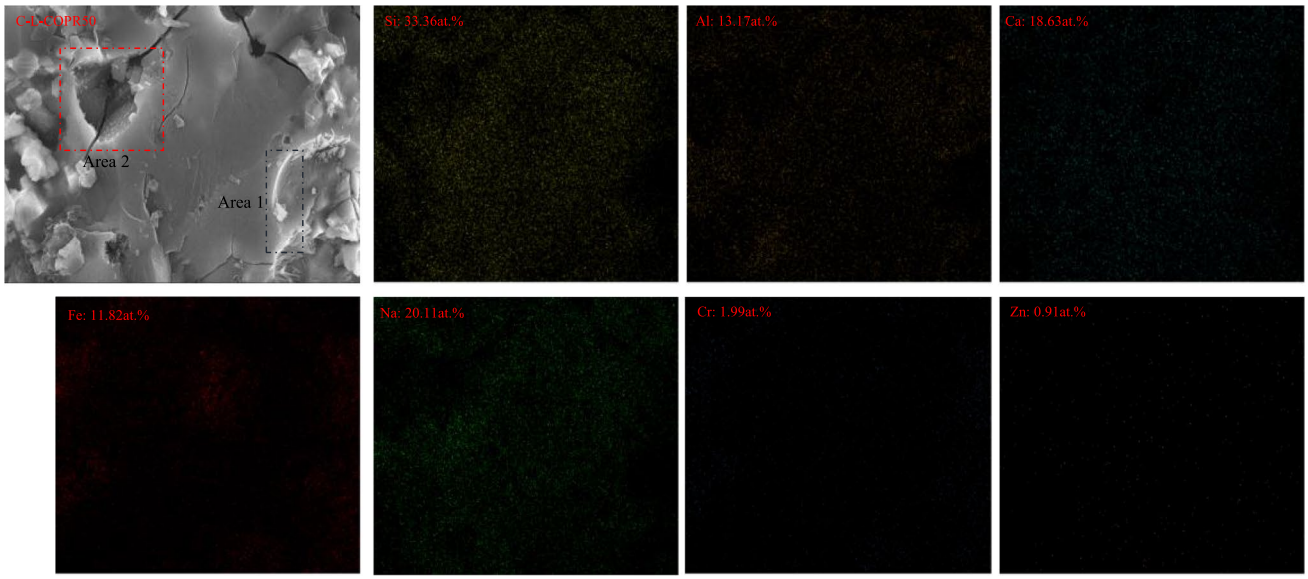

Fig. 13 Microstructure and energy spectrum of C-L-COPR50

of the FA-LZSS-based composite binders. Because the magnitude of the wave number shift can be viewed as the effect of heavy metal ions on the structure of geopolymer gels (Zhang et al. 2008). It is worth noting that the O-C-O tensile vibrations (band "4" in Fig. 12A and the band "d" in Fig. 12B) around 1450 cm^{-1} for all samples become sharper with the addition of COPR. This may be due to the reaction between carbon dioxide retention and alkaline void liquid during the solidification of alkali-activated slurry. The frequency band around 880 cm^{-1} also verified the existence of carbonate (García-Lodeiro et al. 2008).

SEM–EDS analysis

Figures 13 and 14 show the microstructure and energy spectrum analysis of C-L-COPR50 and F-L-COPR50, respectively. The morphology image shows that the spherical particles representing FA are corroded by alkali activation (area 1 and area 4) and are tightly bonded to the gel products. Irregular particles were coated with gel products in area 2 and area 3 regions, which may be incomplete reaction LZSS particles or COPR particles. The composite binder formed a dense gel, which hindered the leaching of heavy metals.

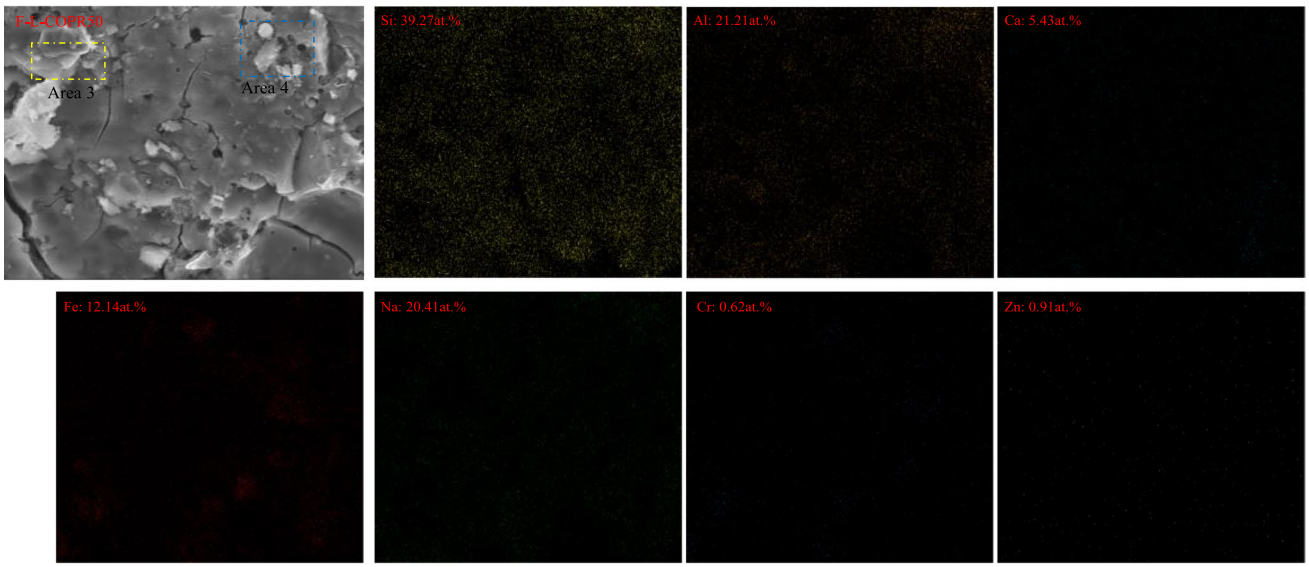

Fig. 14 Microstructure and energy spectrum analysis of F-L-COPR50

Table 7 COPR disposal capacity of various binders

Binders	Max addition of COPR (%)	Compressive strength at 28 days (MPa)	Ref
BFS	70 (50)	13.41 (23.15)	Huang et al. (2016)
BFS + AA[1]	60	0.43	Xia et al. (2020)
BFS + FFA + MK	60 (50)	25.12 (32.34)	Huang et al. (2018)
BFS + RM[2] (3:7)	30	16.58	Luo et al. (2022b)
BFS + RM (4:6)	30	30.04	
BFS + RM (5:5)	30	45.12	
LZSS	40	1.42	Yu et al. (2021)
CFA + LZSS	50	27.27	In this work
FFA + LZSS	50	26.11	In this work

[1]Acetic acid

[2]Red mud

When COPR reached 50%, the heavy metals zinc and chromium could hardly be detected, indicating that the heavy metals were effectively fixed or wrapped.

The EDS analysis of Si, Al, Ca, and Na of C-L-COPR50 shows that they are evenly dispersed in the morphology map, resulting from the coexistence of C-A-S–H, N-A-S–H, and C/N-A-S–H in the composite binder. However, Si, Al, and Na are mainly detected in the energy spectrum of F-L-COPR50, which is related to more quartz crystals and mullite in FFA. According to the distribution of sodium elements in the energy spectrum, it can be inferred that F-L-COPR50 is mainly N-A-S–H gel structure. At the same time, cracks in the microstructure may be caused by stress damage in the sample preparation process. It also characterized the drying shrinkage of the gel, forming a denser structure and reflecting better resistance to chemical corrosion (Ariffin et al. 2013).

Discussion

Composite binders have advantages over single-material binders in stabilizing hazardous wastes. The treatment ability and environmental stability of FA-LZSS-based composite binder for COPR were explored. The previous binders used for COPR disposal are summarized in Table 7. It can be found previous studies mainly focused on blast furnace slag as the basic binder material, which is related to calcium content similar to that of PC. In this study, FA was used as the matrix material, and LZSS was introduced to prepare the composite binder, which improved the ability of COPR disposal and maintained a good compressive strength when the COPR content reached 50 wt% to meet the compressive strength required by construction projects.

The activation products of CFA and FFA used in the experiment are not identical in the composite binder. The mineral phase analysis in Fig. 10 shows that in addition to calcium hydrate, F-L-COPR50 contains N-A-S–H geopolymer gel. This results in the two binders showing different acid corrosion resistance in the semi-dynamic leaching test. The 3D cross-linking structure of N-A-S–H makes it better to solidify and stabilize heavy metals and effectively resist acid corrosion. In contrast, the solubility of calcium hydrates in acidic environments makes them more affected by the environment (Garcia-Lodeiro et al. 2011; Rathee and Singh 2022).

The De value of the experiment reveals that higher calcium hydrate is not conducive to the solidification and stabilization of heavy metals, and the dissolution mechanism occurs in an acidic environment. Therefore, when using a calcium-containing composite binder to solidify and stabilize heavy metals, the calcium content and pH of the alkali activator should be considered in an appropriate range to inhibit more free calcium-containing hydrates (such as $Ca(OH)_2$) and make them produce C-A-S–H gel with a higher degree of polymerization (Guo et al. 2010).

The effective S/S of hexavalent chromium and zinc ions by the composite binder was realized. It was also found that the low-calcium system had more corrosion resistance stability than the high-calcium system. In previous studies, it has been proved that N-A-S–H has higher corrosion resistance than calcium-containing gel. The process of using solid waste to prepare binders differs from traditional cement. It is necessary to compare further and explore the influence of calcium components on the environmental stability of the solidified body.

Conclusions

The alkali activation technique can be used to recycle industrial solid waste into cementitious materials that are equivalent to PC. In this experiment, the capacity of composite binder to deal with COPR is superior to that of the earlier BFS and red mud. Hazardous waste can be treated as general industrial waste after stabilization and solidification and may be used as building materials. Semi-dynamic leaching experiments were used to study the effectiveness of co-immobilization of zinc and hexavalent chromium. The main research conclusions are as follows:

(1) The addition of COPR reduces the mechanical properties of FA-LZSS-based composite binders. When COPR reaches 50%, the solidified body still has a compressive strength of more than 25 MPa, and the mechanical properties are good.
(2) CFA-LZSS and FFA-LZSS composite binders have good immobility ability for heavy metals contained

in COPR. In the simulated landfill leachate and the acid rain environment, the concentration of Cr(VI) and Zn^{2+} was lower than the limits of GB5085.3–2007 and US.EPA.1311. The S/S efficiency of the composite binder for Cr(VI) is better than that of Zn^{2+}.

(3) The ANC test of the solidified body shows that the increase in calcium content will enhance the acid-neutralization ability, and the solubility of calcium hydrate with acid should be fully considered. The more acidic the environment, the higher the leaching concentration of heavy metal ions.

(4) In the semi-dynamic leaching test, the low-calcium system has better environmental stability, and the N-A-S–H gel phase formed has better acid corrosion resistance than calcium hydrate. The higher calcium content may lead to the dissolution mechanism of the solidified body in the environment and the rapid release of heavy metal ions. Binder fixed Zn better than Cr(VI). The leaching of Zn^{2+} is mainly affected by surface washing, and the leaching rate is very low. The leaching of Cr(VI) is mainly controlled by diffusion. The leaching rate of heavy metals is slow and has good environmental stability.

(5) The environmental stability of the composite binder solidified body is good. It has good acid corrosion resistance and even more adequate curing in water environments, and its mechanical properties are maintained. The solubility of calcium hydrate in a high calcium system in an acidic environment should be considered, and the low calcium system has better environmental corrosion resistance.

(6) XRD, FTIR, and SEM–EDS analysis revealed that the main gel products in the composite binder were C-S–H, C-A-S–H, and N-A-S–H. Heavy metals are physically and chemically fixed. The spinel phase (spinel (Zn, Cr-exchanged)) provides chemical sites for the immobilization of Zn and Cr(VI).

Author contribution Guangjun Peng: investigation; methodology; formal analysis; roles/writing—original draft. Pengpeng Zhang: software; writing—review and editing. Linghao Zeng: methodology; formal analysis; validation. Lin Yu: supervision; conceptualization; resources. Dongwei Li: supervision; conceptualization.

Data availability All data generated or analyzed during this study are included in the published article.

Declarations

Ethics approval and consent to participate Not applicable.

Consent for publication Not applicable.

Competing interests The authors declare no competing interests.

References

Agrawal A, Kumar V, Pandey BD (2006) Remediation options for the treatment of electroplating and leather tanning effluent containing chromium—a review. Miner Process Extr Metall Rev 27:99–130. https://doi.org/10.1080/08827500600563319

Ariffin MAM, Bhutta MAR, Hussin MW et al (2013) Sulfuric acid resistance of blended ash geopolymer concrete. Constr Build Mater 43:80–86. https://doi.org/10.1016/j.conbuildmat.2013.01.018

ASTM (2008) Standard test method for accelerated leach test for diffusive releases from solidified waste and a computer program to model diffusive, fractional leaching from cylindrical waste forms. ASTM

Bakharev T (2005) Resistance of geopolymer materials to acid attack. Cem Concr Res 35:658–670. https://doi.org/10.1016/j.cemconres.2004.06.005

Belviso C (2018) State-of-the-art applications of fly ash from coal and biomass: a focus on zeolite synthesis processes and issues. Prog Energy Combust Sci 65:109–135. https://doi.org/10.1016/j.pecs.2017.10.004

Bratovcic A, Buksek H, Helix-Nielsen C, Petrinic I (2022) Concentrating hexavalent chromium electroplating wastewater for recovery and reuse by forward osmosis using underground brine as draw solution. Chem Eng J 431:133918. https://doi.org/10.1016/j.cej.2021.133918

Chao L, Yu L, Sun H, Li L (2011) The composition of fly ash glass phase and its dissolution properties applying to geopolymeric materials. J Am Ceram Soc 94:1773–1778. https://doi.org/10.1111/j.1551-2916.2010.04337.x

Chen EY, Li TZ (2011) The ecological environmental effect of high quality blast furnace slag power. China Concrete 5:24–28

Cho Y-K, Yoo S-W, Jung S-H et al (2017) Effect of Na_2O content, SiO_2/Na_2O molar ratio, and curing conditions on the compressive strength of FA-based geopolymer. Constr Build Mater 145:253–260. https://doi.org/10.1016/j.conbuildmat.2017.04.004

Chrysochoou M, Dermatas D (2006) Evaluation of ettringite and hydrocalumite formation for heavy metal immobilization: literature review and experimental study. J Hazard Mater 136:20–33. https://doi.org/10.1016/j.jhazmat.2005.11.008

Chrysochoou M, Fakra SC, Marcus MA et al (2010) Microstructural analyses of Cr(VI) speciation in chromite ore processing residue (COPR). Environ Sci Technol 43:5461–5466. https://doi.org/10.1021/es9005338

Dermatas D, Moon DH, Menounou N et al (2004) An evaluation of arsenic release from monolithic solids using a modified semi-dynamic leaching test. J Hazard Mater 116:25–38. https://doi.org/10.1016/j.jhazmat.2004.04.023

Du Y, Chrysochoou M (2020) Microstructural analyses of Cr(VI) speciation in chromite ore processing residue from the soda ash process. J Hazard Mater 393:122385. https://doi.org/10.1016/j.jhazmat.2020.122385

Fernández-Jiménez A, Palomo A (2005) Composition and microstructure of alkali activated fly ash binder: effect of the activator. Cem Concr Res 35:1984–1992. https://doi.org/10.1016/j.cemconres.2005.03.003

Gao W, Ni W, Zhang Y et al (2020) Investigation into the semi-dynamic leaching characteristics of arsenic and antimony from solidified/stabilized tailings using metallurgical slag-based binders. J Hazard Mater 381:120992. https://doi.org/10.1016/j.jhazmat.2019.120992

García-Lodeiro I, Fernández-Jiménez A, Blanco MT, Palomo A (2008) FTIR study of the sol–gel synthesis of cementitious gels: C-S–H and N–A–S–H. J Sol-Gel Sci Technol 45:63–72. https://doi.org/10.1007/s10971-007-1643-6

Garcia-Lodeiro I, Palomo A, Fernández-Jiménez A, Macphee DE (2011) Compatibility studies between N-A-S-H and C-A-S-H

gels. Study in the ternary diagram Na_2O–CaO–Al_2O_3–SiO_2–H_2O. Cem Concr Res 41:923–931. https://doi.org/10.1016/j.cemconres.2011.05.006

Görhan G, Kürklü G (2014) The influence of the NaOH solution on the properties of the fly ash-based geopolymer mortar cured at different temperatures. Compos B Eng 58:371–377. https://doi.org/10.1016/j.compositesb.2013.10.082

Guo X, Shi H, Chen L, Dick WA (2010) Alkali-activated complex binders from class C fly ash and Ca-containing admixtures. J Hazard Mater 173:480–486. https://doi.org/10.1016/j.jhazmat.2009.08.110

Huang X, Huang T, Li S et al (2016) Immobilization of chromite ore processing residue with alkali-activated blast furnace slag-based geopolymer. Ceram Int 42:9538–9549. https://doi.org/10.1016/j.ceramint.2016.03.033

Huang X, Muhammad F, Yu L et al (2018) Reduction/immobilization of chromite ore processing residue using composite materials based geopolymer coupled with zero-valent iron. Ceram Int 44:3454–3463. https://doi.org/10.1016/j.ceramint.2017.11.148

Kanchinadham S, Narasimman LM, Pedaballe V, Kalyanaraman C (2015) Diffusion and leachability index studies on stabilization of chromium contaminated soil using fly ash. J Hazard Mater 297(52):58. https://doi.org/10.1016/j.jhazmat.2015.04.045

Komljenović M, Tanasijević G, Džunuzović N, Provis JL (2020) Immobilization of cesium with alkali-activated blast furnace slag. J Hazard Mater 388:121765. https://doi.org/10.1016/j.jhazmat.2019.121765

Li Y-C, Min X-B, Chai L-Y et al (2016) Co-treatment of gypsum sludge and Pb/Zn smelting slag for the solidification of sludge containing arsenic and heavy metals. J Environ Manage 181:756–761. https://doi.org/10.1016/j.jenvman.2016.07.031

Li J, Sun P, Li J et al (2020) Synthesis of electrolytic manganese residue-fly ash based geopolymers with high compressive strength. Construct Build Mater 248:118489. https://doi.org/10.1016/j.conbuildmat.2020.118489

Liu X, Zhao X, Yin H et al (2018) Intermediate-calcium based cementitious materials prepared by MSWI fly ash and other solid wastes: hydration characteristics and heavy metals solidification behavior. J Hazard Mater 349:262–271. https://doi.org/10.1016/j.jhazmat.2017.12.072

Luo S, Zhao S, Zhang P et al (2022a) Co-disposal of MSWI fly ash and lead–zinc smelting slag through alkali-activation technology. Construct Build Mater 327:127006. https://doi.org/10.1016/j.conbuildmat.2022.127006

Luo Z, Zhi T, Liu L et al (2022b) Solidification/stabilization of chromium slag in red mud-based geopolymer. Construct Build Mater 316:125813. https://doi.org/10.1016/j.conbuildmat.2021.125813

Majee S, Halder G, Mandal DD et al (2021) Transforming wet blue leather and potato peel into an eco-friendly bio-organic NPK fertilizer for intensifying crop productivity and retrieving value-added recyclable chromium salts. J Hazard Mater 411:125046. https://doi.org/10.1016/j.jhazmat.2021.125046

Malviya R, Chaudhary R (2006) Leaching behavior and immobilization of heavy metals in solidified/stabilized products. J Hazard Mater 137:207–217. https://doi.org/10.1016/j.jhazmat.2006.01.056

Muhammad F, Xia M, Li S et al (2019) The reduction of chromite ore processing residues by green tea synthesized nano zerovalent iron and its solidification/stabilization in composite geopolymer. J Clean Prod 234:381–391. https://doi.org/10.1016/j.jclepro.2019.06.004

Nath SK (2019) Fly ash and zinc slag blended geopolymer: immobilization of hazardous materials and development of paving blocks. J Hazard Mater 387:121673. https://doi.org/10.1016/j.jhazmat.2019.121673

Pacheco-Torgal F, Castro-Gomes J, Jalali S (2008) Alkali-activated binders: a review. Part 1. Historical background, terminology, reaction mechanisms and hydration products. Construct Build Mater 22:1305–1314. https://doi.org/10.1016/j.conbuildmat.2007.10.015

Fernández-Jiménez A, Palomo A (2003) Characterisation of fly ashes. Potential reactivity as alkaline cements☆. Fuel 82:2259–2265. https://doi.org/10.1016/S0016-2361(03)00194-7

Poon CS, Wong YL, Lam L (1997) The influence of different curing conditions on the pore structure and related properties of fly-ash cement pastes and mortars. Constr Build Mater 11:383–393. https://doi.org/10.1016/S0950-0618(97)00061-5

Pt A, Cg B, Sj C (2008) Alkali-activated binders: a review. Part 2. About materials and binders manufacture. Constr Build Mater 22:1315–1322. https://doi.org/10.1016/j.conbuildmat.2007.03.019

Rathee M, Singh N (2022) Durability properties of copper slag and coal bottom ash based I-shaped geopolymer paver blocks. Construct Build Mater 347:128461. https://doi.org/10.1016/j.conbuildmat.2022.128461

Rha CY, Kang SK, Kim CE (2000) Investigation of the stability of hardened slag paste for the stabilization/solidification of wastes containing heavy metal ions. J Hazard Mater 73:255–267. https://doi.org/10.1016/S0304-3894(99)00185-5

Salihoglu G (2014) Immobilization of antimony waste slag by applying geopolymerization and stabilization/solidification technologies. J Air Waste Manag Assoc 64:1288–1298. https://doi.org/10.1080/10962247.2014.943352

Shanker AK, Venkateswarlu B (2011) Chromium: environmental pollution, health effects and mode of action. Enc Environ Health 650–659. https://doi.org/10.1016/B978-0-444-52272-6.00390-1

Shi C, Fernández-Jiménez A (2006) Stabilization/solidification of hazardous and radioactive wastes with alkali-activated cements. J Hazard Mater 137:1656–1663. https://doi.org/10.1016/j.jhazmat.2006.05.008

Singh TS, Pant KK (2006) Solidification/stabilization of arsenic containing solid wastes using portland cement, fly ash and polymeric materials. J Hazard Mater 131:29–36. https://doi.org/10.1016/j.jhazmat.2005.06.046

Song F, Gu L, Zhu N, Yuan H (2013) Leaching behavior of heavy metals from sewage sludge solidified by cement-based binders. Chemosphere 92:344–350. https://doi.org/10.1016/j.chemosphere.2013.01.022

Stegemann J, Côté P (1999) Investigation of test methods for solidified waste evaluation — a cooperative program. Report Eps

Sun Y, Du Y, Lan J et al (2021) A new method (ball milling and sodium sulfide) for mechanochemical treatment of soda ash chromite ore processing residue. J Hazard Mater 415:125601. https://doi.org/10.1016/j.jhazmat.2021.125601

Tang Y, Wang Y, Huan B et al (2017) Leachability of hazardous trace elements from entrained-flow coal gasification residues in Ningdong, China. Energy Fuels 31:9703–9716. https://doi.org/10.1021/acs.energyfuels.7b01338

UNE-EN 12457-4-2003 (2003) Characterisation of waste - Leaching - Compliance test for leaching of granular waste materials and sludges - Part 4: One stage batch test at a liquid to solid ratio of 10 l/kg for materials with particle size below 10 mm (without or with size reduction) [S]

Wang Y, Han F et al (2018) Solidification/stabilization mechanism of Pb(II), Cd(II), Mn(II) and Cr(III) in fly ash based geopolymers. Constr Build Mater 160:818–827. https://doi.org/10.1016/j.conbuildmat.2017.12.006

Wang G, Ning X, Lu X et al (2019) Effect of sintering temperature on mineral composition and heavy metals mobility in tailings bricks.

Waste Manage 93:112–121. https://doi.org/10.1016/j.wasman.2019.04.001

Xia M, Muhammad F, Zeng L et al (2019) Solidification/stabilization of lead-zinc smelting slag in composite based geopolymer. J Clean Prod 209:1206–1215. https://doi.org/10.1016/j.jclepro.2018.10.265

Xia M, Muhammad F, Zhao S et al (2020) Detoxification and immobilization of chromite ore processing residue using the alkali-activated cementitious materials mixed with ascorbic acid. J Environ Manag 265:110350. https://doi.org/10.1016/j.jenvman.2020.110350

Yip CK, Lukey GC, Provis JL, Deventer J (2008) Effect of calcium silicate sources on geopolymerisation. Cem Concr Res 38:554–564. https://doi.org/10.1016/j.cemconres.2007.11.001

Yu Q, Li H, Zheng Y et al (2022) Promoted electrokinetic treatment of Cr from chromite ore processing residue with rhamnolipid: focusing on the reactions on electrolyte-residue interfaces. J Environ Chem Eng 10:106954. https://doi.org/10.1016/j.jece.2021.106954

Yu L, Fang L, Zhang P et al (2021) The utilization of alkali-activated lead–zinc smelting slag for chromite ore processing residue solidification/stabilization. Int J Environ Res Public Health 18. https://doi.org/10.3390/ijerph18199960

Zhang J, Provis JL, Feng D, van Deventer JSJ (2008) Geopolymers for immobilization of Cr^{6+}, Cd^{2+}, and Pb^{2+}. J Hazard Mater 157:587–598. https://doi.org/10.1016/j.jhazmat.2008.01.053

Zhang Z, Provis JL, Reid A, Wang H (2014) Fly ash-based geopolymers: the relationship between composition, pore structure and efflorescence. Cem Concr Res 64:30–41. https://doi.org/10.1016/j.cemconres.2014.06.004

Zhang P, Muhammad F, Yu L et al (2020) Self-cementation solidification of heavy metals in lead-zinc smelting slag through alkali-activated materials. Construct Build Mater 249:118756. https://doi.org/10.1016/j.conbuildmat.2020.118756

Note on preprint server I have not submitted my manuscript to a preprint server before submitting it to Environmental Science and Pollution Research.

Publisher's note Springer Nature remains neutral with regard to jurisdictional claims in published maps and institutional affiliations.